REVIEW ARTICLE

Technical Aspects: Image Reconstruction

Masahisa Onoguchi, RT, PhD[1)], Takahiro Konishi, RT, MS[2)], Takayuki Shibutani, RT, MS[1)], Shinro Matsuo, MD, PhD[3)] and Kenichi Nakajima, MD, PhD[3)]

Received: May 14, 2016/Revised manuscript received: July 25, 2016/Accepted: July 26, 2016

Abstract

Recent developments in nuclear medicine technology have been remarkable, with new technologies emerging in both hardware and software. In this study, we focused on an image reconstruction method known as the ordered subset conjugate gradient minimizer (OSCGM) method. We conducted a myocardial phantom experiment and a clinical study to examine the difference between this technology and conventional methods as well as the characteristics of an IQ-SPECT system with this technology. The outline is shown.
Keywords: Image Reconstruction, IQ-SPECT, Myocardial phantom, OSCGM
Ann Nucl Cardiol 2016；2（1）：68-72

The IQ-SPECT System (SIEMENS, Germany) was recently introduced for short-term acquisition of myocardial perfusion scintigraphy. It uses the same SPECT acquisition technique using Anger-type gamma camera technology as conventional methods, at the same time, this system comprises three technologies: a SMARTZOOM collimator, rotational orbit around the center of the heart, and the OSCGM method.

The first technology, the SMARTZOOM collimator, contains a region called the sweet spot, which has the highest count rate for magnification and sensitivity at 28 cm from the collimator, enabling expanded acquisition of the heart. The second technology, the rotational orbit of the heart's center, enables the imaging of a heart within the sweet spot from any acquisition view (expanding the heart by a zoom factor of 2 and preventing truncation in myocardial marginal regions). The third technology is the induction of the OSCGM method. Equipped with these three technologies, this is an imaging system that considerably shortens the acquisition time to 1/4 of that of conventional methods and allows low-dose imaging protocols (1,2).

From the FBP and OS-EM methods to the OSCGM method

Nuclear medicine images suffer from noise statistics; in particular, the resolution and quantitation are affected by the absorption and scatter of gamma rays. For image reconstruction of projection data into tomographic images, various technologies have been developed and implemented to solve the above problems. There are two main methods for image reconstruction in nuclear medicine. One is the filtered buck-projection (FBP) method (3), which has been used for a long time. It is difficult for this method to obtain true radioactivity, owing to effects such as statistical noise, response characteristics of the detector, attenuation and scatter. The other method is iterative reconstruction. This method requires a high amount of computation but has recently been implemented following the development of high-speed and advanced computers. Iterative reconstruction can make corrections for resolution, scattering, and attenuation by incorporating possible physical phenomenon into the diagnostic system in the process of image reconstruction. Techniques such as maximum likelihood-expectation maximization (ML-EM) (4) and its high-speed variant, ordered subset-expectation maximization

doi：10.17996/ANC.02.01.68

1) Masahisa Onoguchi, Takayuki Shibutani
Department of Quantum Medical Technology, Institute of Medical, Pharmaceutical and Health Sciences, Kanazawa University, 5-11-80 Kodatsuno, Kanazawa, Ishikawa, Japan 920-0942
E-mail: onoguchi@staff.kanazawa-u.ac.jp
2) Takahiro Konishi
Department of Radiology, Kanazawa University Hospital, Kanazawa, Ishikawa, Japan
3) Shinro Matsuo, Kenichi Nakajima
Department of Nuclear Medicine, Kanazawa University Hospital, Kanazawa, Ishikawa, Japan

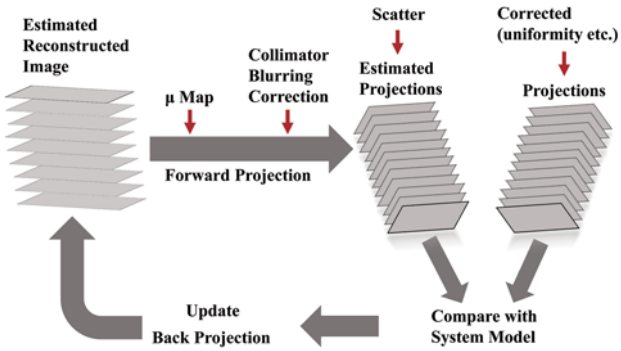

Fig. 1 The concept of the OSEM method

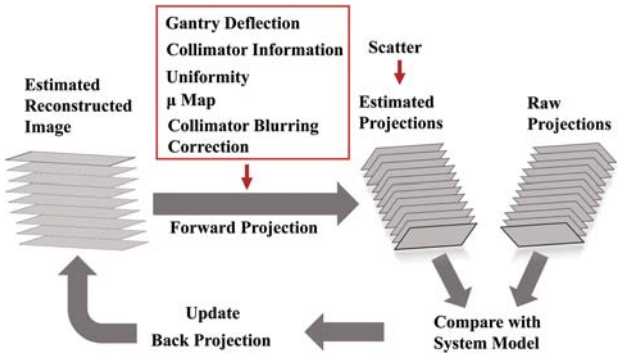

Fig. 2 The concept of the OSCGM method

(OS-EM) (5), have attracted attention for this method. For iterative reconstruction by which many corrections are possible, the main response function is collimator blurring correction such as the depth dependent isotropic resolution recovery. In the FBP method, there is no collimator blurring correction and a pencil beam is the basis. FBP is based on an assumption that every projection data was created with pencil beam. A 2D-OSEM method performs collimator blurring correction using the fan-beam model of a slice cross-section. Recently, a 3D-OSEM method has been developed, which can offer focus correction for the source-collimator distance, enabling a three-dimensional beam model for collimator blurring correction including that of the axis direction. This development has contributed to further improvement in image quality. The introduction of iterative reconstruction with this resolution correction has led to improvements in the spatial resolution, contrast, and diagnostic accuracy, and to short-time acquisition (6), offering further improvements on the FBP method. However, the collimator blurring correction only corrects blur owing to the collimator (e.g., thickness, hole diameter, etc.) and does not improve the resolution of the detector itself.

Recently, a new image reconstruction method with a more advanced model based on the 3D-OSEM method, an ordered subset conjugate gradient minimizer (OSCGM) method, has been developed. This OSCGM can make corrections in the process of image reconstruction using data from close-to-actual-measurements such as the shape and distortion of the collimator hole or the bend in the gantry. In contrast, the amount of data is large, and the conventional 3D-OSEM methods take a long time for conversion; thus, the conjugate gradient method is used for its fast convergence.

Difference between the OSEM and OSCGM methods

Fig. 1 shows the concept of the OSEM method. First, the volume data of the photo peak tomographic image is estimated. Next, the detection probabilities incorporating physical phenomenon in the diagnostics system, such as attenuation and blur due to the collimator aperture, are considered for estimating the projection data by forward projection. These estimated data are compared with the actually measured projection of the main peak. These projection data of the main peak include scatter; thus, a scatter component is added to the estimated projection data. By comparing the two datasets, only the photo peak data are updated, since the scatter component comprises actually measured data. This process is repeated until the true values are reached. Fig. 2 shows the concept of the OSCGM method. This method is basically the same as OSEM. The difference is that the conventional methods apply corrections such as for uniformity to the measured projection data and conduct image reconstruction by comparison. During image reconstruction, the OSCGM method does not compare with the corrected data but instead incorporates, during comparison with the raw data, factors such as corrections for uniformity, collimator-hole shape, distortion, gantry bend, and time lag in rotation. The specific differences are the following three points: 1) Conventionally, the point-spread function (PSF) of the Gaussian distribution is calculated based on the geometric structure of the collimator hole and used as the resolution-correction information. With the SMARTZOOM collimator (radius of rotation 28 cm, fixed), however, high accuracy has been achieved by changing the PSF from a Gaussian function to a hexagonal shape identical to the collimator hole. 2) This method measures deviation differences between the design and actual structures caused during collimator manufacturing, and corrects the precision error of the collimator. 3) This method models the gantry bend in 3D rotation instead of 2D and corrects the detector-location information to within 0.1 mm and 0.1 °, improving the resolution reduction caused by the rotating detector. A conjugate gradient method is necessary to make the above differences possible. This is because the correction amount is large, the geometry is complex, and incorporating vector maps, which are close to reality, makes the amount of data large; thus, reconstruction is extremely time consuming just by the OSEM method. Therefore, the OSCGM method is applied for convergence (7). Although the OSCGM method can converge relatively faster,

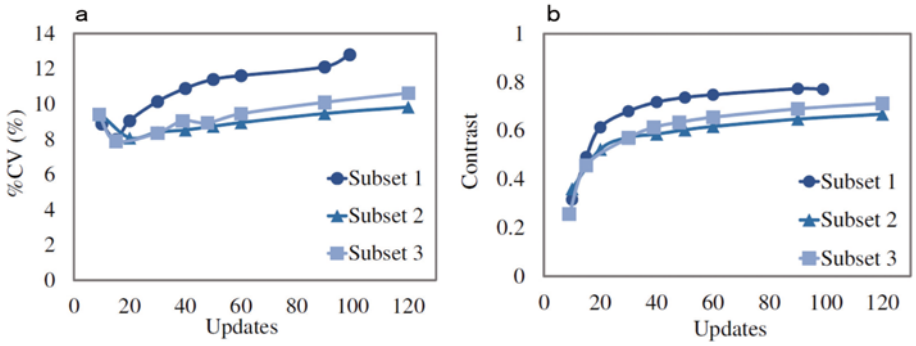

Fig. 3　a: The relationship between update and %CV for ^{99m}Tc.
b: The relationship between update and contrast for ^{99m}Tc.

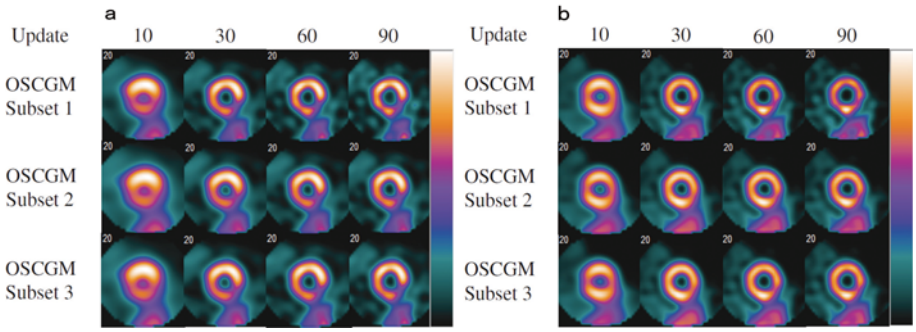

Fig. 4　a: ^{99m}Tc IQ-SPECT image without correction.
b: The images (middle slice) to attenuation and scatter correction (ACSC).

it is sensitive to noise, so Mighell's modified Chi-squared evaluation is applied to the merit function (function to measure between the projected and real measured data) to prevent noise and build-up.

Myocardial phantom

The characteristics of images from myocardial phantom with no defect experiments with ^{201}TlCl (^{201}Tl) and ^{99m}Tc using the IQ-SPECT system are described below.

For the physical evaluation, the relationship among update (subset number × iteration number), %CV, and contrast data for ^{99m}Tc are described. The characteristics of the SPECT images of ^{99m}Tc and ^{201}Tl are used for visual evaluation. The acquisition conditions of the SMARTZOOM collimator for ^{99m}Tc are as follows: matrix 128 × 128; projection number 34; acquisition time 9 sec/view; rotational angle 208 °; radius of rotation 28 cm from the heart center; a zoom factor of 1; main window 141 keV ± 10%; sub-window upper lower 20%. For ^{201}Tl, the acquisition time is 14 sec/view, the main window is 70 keV ± 10%, and the other conditions are same as for ^{99m}Tc.

Fig. 3a shows the relationship between update and %CV for ^{99m}Tc. The horizontal axis denotes the update, whereas the vertical axis denotes %CV. For physical evaluation, %CV deteriorates with increasing update. For the same update, %CV is the same for subsets 1, 2 and 3 but slightly higher for subset 1. Fig. 3b shows the relationship between update and contrast for ^{99m}Tc. Contrast rapidly increases with update up to 30 but slows down afterward. Similar to the results for uniformity, for the same update, contrast is the same for subset 2 and 3 but slightly higher for subset 1.

Fig. 4a shows a ^{99m}Tc IQ-SPECT image without correction, and Fig. 4b shows the images (middle slice) to attenuation and scatter correction (ACSC). From the top, the images were reconstructions of subsets 1, 2, and 3 of the OSCGM and the update was changed from 10 to 90 from left to right. For visual evaluation, as shown in the physical evaluation, image quality significantly increases with increasing update up to 30, but for subsets 2 and 3, a further increase in the update does not alter the image significantly. In contrast, for subset 1, non-uniformity and distortion of myocardium becomes apparent with increasing update. In comparison with the conventional method, for every subset, there is a false defect in the infero-lateral wall, but it is improved by the attenuation correction. As for the image characteristics, there is a false defect in the infero-lateral wall, but this may be because of a shift in the sweet spot center.

Fig. 5a shows the image of ^{201}Tl IQ-SPECT without correction, and Fig. 5b shows the image (middle slice) with attenuation and scatter correction (ACSC). Similar to ^{99m}Tc, the image significantly changes with increasing update up to 30. The distribution of the infero-lateral wall is also reduced; in particular, the deterioration of the image with increasing update becomes more apparent than it does for ^{99m}Tc in subset

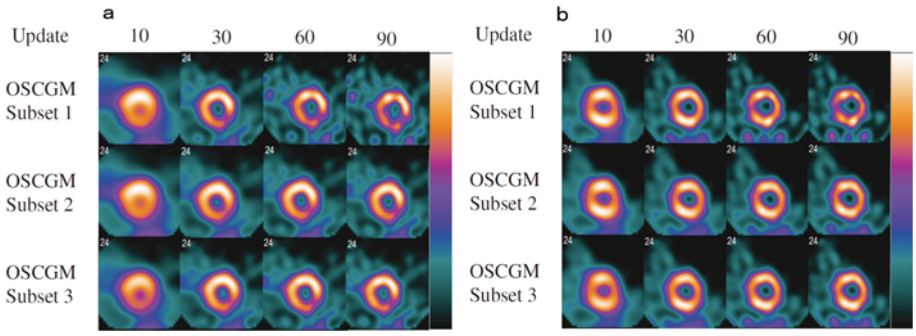

Fig. 5 a: The image of ^{201}Tl IQ-SPECT without correction.
b: The image (middle slice) with attenuation and scatter correction (ACSC).

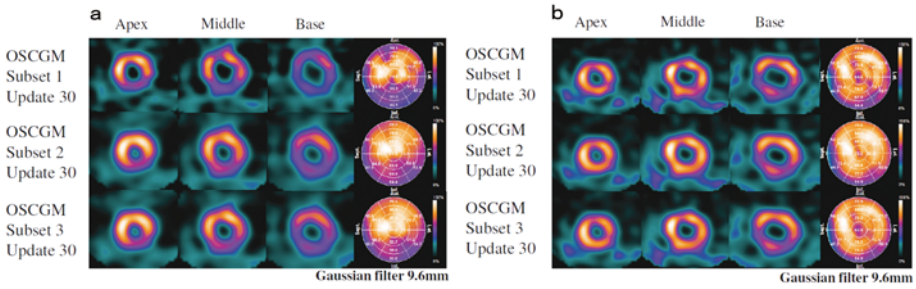

Fig. 6 a: The subset number, short-axis image, and Bull's eye map of ^{201}Tl IQ-SPECT without correction.
b: The ^{201}Tl IQ-SPECT with attenuation and scatter correction (ACSC).

1. A false defect in the infero-lateral wall is also observed, though not as strongly as for ^{99m}Tc. The images for subsets 2 and 3 for the same numbers are equivalent. For attenuation and scatter correction (ACSC) similar to the case of ^{99m}Tc, the myocardial distribution becomes uniform after correction. For subset 1, however, distortion and non-uniformity of the myocardium become apparent with increasing update. The results of the phantom study indicate that the convergence is faster than that of the conventional OSEM with resolution correction and the optimal number of updates is approximately 30. As for the image characteristics, there is a false defect in the infero-lateral wall, but this may be because of a shift in the sweet spot center as same as ^{99m}Tc which might be improved by attenuation correction. Furthermore, subsets 2 and 3 result in almost the same images at the same update number, but for subset 1, the defect and distortion are prominent and prevent the appearance of the same image, even at the same update.

Normal clinical study

We describe characteristics of the images of a normal subject by IQ-SPECT system with ^{201}Tl myocardial perfusion scintigraphy. The acquisition conditions are the same as those used in the phantom study. Fig. 6a shows the subset number, short-axis image, and Bull's eye map of ^{201}Tl IQ-SPECT without correction, and Fig. 6b shows the image with attenuation and scatter correction (ACSC). With an update number of 30, subsets 1, 2, and 3 correspond to the image reconstruction slices at the apex portion, middle portion, and base portion, respectively. Similar to the phantom experiment, without correction, the defect and image distortion are prominent for subset 1 in the clinical study. Furthermore, there are false defects in the septum and inferior wall close to the anterior wall. The images of subsets 2 and 3 are similar. In the attenuation and scatter correction images, the false defect in the infero-lateral wall is improved by attenuation correction, but this correction in turn reduces the distribution of the apex portion. Compared with subsets 2 and 3, subset 1 had a prominent distortion and non-uniformity in the myocardium.

As shown above, the introduction of the OSCGM method enables the incorporation of a high-accuracy model and measured data into reconstruction. The IQ-SPECT system uses the OSCGM method and incorporates highly accurate correction data into reconstruction and uses an acquisition method appropriate for the model, realizing diagnostic performance equivalent to the conventional method with a shorter acquisition time.

However, the images produced by the IQ-SPECT system have different characteristics from those of the conventional method. Moreover, interpretation of the IQ-SPECT system's images is difficult because they are still unfamiliar. It is therefore considered necessary to improve defects in the infero-lateral wall and use a normal database to supplement the interpretation.

Potential and prospects of the OSCGM method

In this study we showed the characteristics of the OSCGM method used by IQ-SPECT. This method is also used in xSPECT (SIEMENS). However, the OSCGM method in xSPECT is a different model from that in IQ-SPECT, and measured values with consideration of the penetration and scattering on the partition wall are used for the PSF (8). In other words, the PSF in IQ-SPECT uses hexagonal approximation data, while that in xSPECT uses measured values, enabling more accurate resolution correction. Moreover, the recently-developed Q. Clear (GE Healthcare) uses a block-sequential regularized expectation maximization (BSREM) reconstruction algorithm (9). Unlike the OSEM method, the BSREM method makes a 100% convergence in the voxel unit on the image; thus, it does not require input of subsets or iteration. Furthermore, image noises are controlled in the normalized part in the iterative approximation reconstruction, so that the method does not require post-processing. Recently, two vendors have introduced novel scanners: Discovery NM530c (D530c); GE Healthcare and D-SPECT; Spectrum Dynamics utilizing the same cadmium zinc-telluride (CZT) detectors, with a different combination of high-sensitivity multipinhole or parallel-hole collimator which focuses on the myocardium (10,11). Miyagawa et al. discussed the semiconductor SPECT is also another approach to improve the image quality, and then the total effective dose （stress and rest） decreased from 9.3 mSv in the 4 MBq/kg group to 5.8 mSv in the 2.5 MBq/kg group (12).

In the future, further improvement in the accuracy of quantitative measurement will lead to higher quantitative of SPECT using a more advanced model. This will find applications not only in the screening of tumors but also in various fields such as differentiation of degenerative diseases and treatment monitoring.

Acknowledgment

The data presented in this article are partly based on collaborative research work with Siemens Japan (Tokyo, Japan).

Sources of funding

None

Conflicts of interest

None

Reprint requests and correspondence:
Masahisa Onoguchi, RT, PhD
Department of Quantum Medical Technology, Institute of Medical, Pharmaceutical and Health Sciences, Kanazawa University, 5-11-80 Kodatsuno, Kanazawa, Ishikawa, Japan 920-0942
E-mail: onoguchi@staff.kanazawa-u.ac.jp

References

1. Rajaram R, Bhattacharya M, Ding X, et al. IEEE nuclear science symposium conference record 2011.
2. Caobelli F, Ren Kaiser S, Thackeray JT, et al. The importance of a correct positioning of the heart using IQ-SPECT system with multifocal collimators in myocardial perfusion imaging: a phantom study. J Nucl Cardiol 2015; 22: 971-4.
3. Ramachandran GN, Lakshminarayanan AV. Three-dimensional reconstruction from radiographs and electron micrographs: application of convolutions instead of Fourier transforms. Proc Natl Acad Sci USA 1971; 68: 2236-40.
4. Lange K, Carson R. EM reconstruction algorithms for emission and transmission tomography. J Comput Assist Tomogr 1984; 8: 306-16.
5. Hudson HM, Larkin RS. Accelerated image reconstruction using ordered subsets of projection data. IEEE Trans Med Imaging 1994; 13: 601-9.
6. Okuda K, Nakajima K, Yamada M, et al. Optimization of iterative reconstruction parameters with attenuation correction, scatter correction and resolution recovery in myocardial perfusion SPECT/CT. Ann Nucl Med 2014; 28: 60-8.
7. Vija AH, Malmin R, Yahil A, et al. A method for improving the efficiency of myocardial perfusion imaging using conventional SPECT and SPECT/CT imaging systems. 978-1-4244-9106-3/10. 2010 IEEE.
8. Vija AH. SIEMENS White Paper. IQ-SPECT: a technical and clinical overview.
9. Ahn S, Fessler JA. Globally convergent image reconstruction for emission tomography using relaxed ordered subsets algorithms. IEEE Trans Med Imaging 2003; 22: 613-26.
10. Bocher M, Blevis IM, Tsukerman L, et al. A fast cardiac gamma camera with dynamic SPECT capabilities: Design, system validation and future potential. Eur J Nucl Med Mol Imaging 2010; 37: 1887-902.
11. Patton J, Slomka P, Germano G, et al. Recent technologic advances in nuclear cardiology. J Nucl Cardiol 2007; 14: 501-13.
12. Miyagawa M, Nishiyama Y, Tashiro R, et al. Novel cardiac SPECT technology with semiconductor detectors: Emerging trends and future perspective. Ann Nucl Cardiol 2015; 1(1): 18-26.